

A COMPUTER-ASSISTED PROOF FOR Σ_3 -CHAOS IN THE FORCED DAMPED PENDULUM EQUATION*

BALÁZS BÁNHÉLYI [†], TIBOR CSENDES [‡], BARNABAS M. GARAY [§], AND
LÁSZLÓ HATVANI [¶]

Abstract. The present paper is devoted to studying Hubbard’s pendulum equation

$$\ddot{x} + 10^{-1}\dot{x} + \sin(x) = \cos(t).$$

By rigorous/interval methods of computation, the main assertion of Hubbard on chaos properties of the induced dynamics is lifted from the level of experimentally observed facts to the level of a theorem completely proved. A distinguished family of solutions is shown to be chaotic in the sense that on consecutive time intervals $(2k\pi, 2(k+1)\pi)$ ($k \in \mathbb{Z}$) individual members of the family can freely “choose” between the following possibilities: the pendulum either crosses the bottom position exactly once clockwise or does not cross the bottom position at all or crosses the bottom position exactly once counterclockwise. The proof follows the topological index/degree approach by Mischaikow, Mrozek, and Zgliczynski. The novelty is a definition of the transition graph for which the periodic orbit lemma, the key technical result of the approach aforementioned, turns out to be a consequence of Brouwer’s fixed point theorem. The role of wholly automatic versus ‘trial and error with human overhead’ computer procedures in detecting chaos is also discussed.

Key words. forced damped pendulum, Σ_3 -chaos, computer-aided proof, transition graph, interval arithmetic

AMS subject classifications. 34C28, 37D45, 70K40, 70K55, 65G30

1. Introduction and the main results. The complexity of the solutions to the forced damped pendulum equation

$$m\ell\ddot{x} + b\dot{x} + mg \sin(x) = A \cos(\omega t)$$

and of the related systems is one of the most frequently studied problems in dynamics. For certain values of the parameters, small perturbation results for chaos apply.

However, a purely theoretical approach can hardly lead to a proof for chaos if small perturbation methods break down, in particular, in the special case

$$(1.1) \quad \ddot{x} + 10^{-1}\dot{x} + \sin(x) = \cos(t)$$

(i.e., for parameters $m\ell = mg = A = \omega = 1$ and $b = 10^{-1}$) investigated by Hubbard [20]. Based on numerical experiments and the accompanying abstract considerations mimicking Smale’s geometric horseshoe construction, Hubbard [20] has made the existence of Σ_3 -chaos—both on Poincaré sections of the 2π -solution mapping and also in more natural terms of the dynamics—very plausible. His main result can be restated as follows.

*This work was supported by the Hungarian National Science Foundation Grants OTKA No. T 048377, T 046822, T037491, and T049516.

[†]Institute of Informatics, University of Szeged, H-6701 Szeged P.O. Box 652, Hungary (banhelyi@inf.u-szeged.hu).

[‡]Institute of Informatics, University of Szeged, H-6701 Szeged P.O. Box 652, Hungary (csendes@inf.u-szeged.hu).

[§]Department of Mathematics, Budapest University of Technology, H-1521 Budapest, Hungary and Computer and Automation Institute (SZTAKI), Hungarian Academy of Sciences, H-1111 Budapest, Hungary (garay@math.bme.hu).

[¶]Bolyai Institute of Mathematics, University of Szeged, H-6701 Szeged P.O. Box 428, Hungary (hatvani@math.u-szeged.hu).

THEOREM H (J.H. Hubbard [20]). *Suppose we are given a biinfinite sequence $\{\varepsilon_k\}_{k \in \mathbf{Z}} \in \{-1; 0; 1\}^{\mathbf{Z}}$ arbitrarily chosen. Then the pendulum governed by equation (1.1) has at least one motion that corresponds to the biinfinite sequence $\{\varepsilon_k\}_{k \in \mathbf{Z}}$ in the sense that, during the time interval $(2k\pi, 2(k+1)\pi)$, the pendulum*

- *crosses the bottom position exactly once clockwise if and only if $\varepsilon_k = -1$,*
 - *does not cross the bottom position at all if and only if $\varepsilon_k = 0$,*
 - *crosses the bottom position exactly once counterclockwise if and only if $\varepsilon_k = 1$,*
- and does not point downwards at the time instants $t = 2k\pi$, $k \in \mathbf{Z}$.*

THE FIRST AIM OF THE PRESENT PAPER is to interpret Hubbard's observation within the Mischaikow-Mrozek framework of computer-assisted proofs for horseshoe-type chaos. We use the word 'observation' because as it is written on page 755 of [20], "no statement is proved anywhere". Hubbard arranges numerical evidence according to the framework of symbolic dynamics. We complete his work by filling all gaps via refining some of his theoretical arguments (in particular, by introducing the small quadrangles L_ℓ, M_ℓ, R_ℓ , $\ell \in \mathbf{Z}$) and performing the rigorous interval arithmetics computations necessary. We derive Theorem H as a consequence of a technical result formulated on the basis of Figure 10 in Hubbard [20] portraying images and preimages of three large quadrangles, the convex hulls of the smaller sets $L_\ell \cup M_\ell \cup R_\ell$, $\ell = -1, 0, 1$. In short, the observation is made a theorem.

THEOREM 1.1. *There exist compact pairwise disjoint quadrangles*

$$L_0, M_0, R_0 \subset \{(x, \dot{x}) \in \mathbf{R}^2 \mid 0 < x < 2\pi\}$$

with the properties as follows. Given a biinfinite sequence $\{\varepsilon_k\}_{k \in \mathbf{Z}} \in \{-1; 0; 1\}^{\mathbf{Z}}$, there exists a solution $x = x(\{\varepsilon_k\}_{k \in \mathbf{Z}}) : \mathbf{R} \rightarrow \mathbf{R}$ to equation (1.1) such that

$$(1.2) \quad (x(2k\pi), \dot{x}(2k\pi)) \in \begin{cases} L_{\sigma_k} & \text{if } \varepsilon_k = -1 \\ M_{\sigma_k} & \text{if } \varepsilon_k = 0 \\ R_{\sigma_k} & \text{if } \varepsilon_k = 1 \end{cases}$$

where $\sigma_{k+1} = \sigma_k + \varepsilon_k$, $k \in \mathbf{Z}$ with $\sigma_0 = 0$ and

$$(1.3) \quad L_\ell = L_0 + (2\ell\pi, 0), \quad M_\ell = M_0 + (2\ell\pi, 0), \quad R_\ell = R_0 + (2\ell\pi, 0), \quad \ell \in \mathbf{Z}.$$

Property (1.2) means that the horizontal $2\ell\pi$ -translates L_ℓ, M_ℓ, R_ℓ of the distinguished quadrangles L_0, M_0, R_0 are visited by trajectories of the Poincaré mapping

$$\Pi : \mathbf{R}^2 \rightarrow \mathbf{R}^2, \quad (x(0), \dot{x}(0)) \rightarrow (x(2\pi), \dot{x}(2\pi))$$

in the given order prescribed by the biinfinite sequence $\{\varepsilon_k\}_{k \in \mathbf{Z}}$. The underlying circle of abstract topological results on transition graphs and iterates of continuous mappings is the most important part of the landmark paper by Mischaikow and Mrozek [25] and of the great number of contributions that followed. The essence of the Mischaikow-Mrozek approach is to prove the existence of an abundance of combinatorially different periodic orbits and then, by using the density of periodic orbits in the shift dynamics, to pass to the existence of horseshoe-type chaos. The key technical tool is represented by what we state as Lemma 2.1 in Section 2 below. Lemma 2.1 concerns transition graphs and periodic orbits in two dimension and constitutes the main step in proving Theorem 1.1.

THE SECOND AIM OF THE PRESENT PAPER is to give an elementary proof to a higher-dimensional generalization of Lemma 2.1. Higher dimensional versions of

Lemma 2.1 were given by Gidea and Zgliczynski [17] and Pireddu and Zanolin [32]. The underlying definitions of the transition graphs in [17] and [32] (the latter motivated by [21]) are different. Both proofs are based on Brouwer degree arguments. We give a third definition of the transition graph in higher dimension—the two-dimensional case was settled by Papini and Zanolin [29]—for which a simple application of Brouwer’s fixed point theorem suffices. This implies, in particular, that in some of the earliest computer-assisted proofs for horseshoe-type chaos [25], [45], [46], [47], Conley index and/or Brouwer degree arguments can be replaced by applications of Brouwer’s fixed point theorem. Actually, as it is discussed in Remark 1, it is Miranda theorem (the intermediate value theorem in \mathbb{R}^N , a particularly appealing reformulation of Brouwer’s fixed point theorem) that applies more easily. The ‘rectangular character’ of Miranda theorem fits beautifully to the rectangles in defining the transition graph as well as to the rectangles in rigorous/interval computation.

The computer-aided parts of the proofs of Theorems 1.1 and H were performed both in the LINUX and in the Cygwin environment, on an average personal computer. We used the C-XSC [23] programming language supporting interval arithmetics and the Validated Numerical ODE (VNODE) package by Ned Nedialkov [27], [28]. Our basic references for rigorous/interval computation and set-valued numerics are [1] and [10], respectively.

THE PRESENT PAPER IS ORGANIZED AS FOLLOWS. Section 2 begins with the definition of the transition graph in two dimension, goes on with stating Lemma 2.1, and ends with the proof of Theorem 1.1. TheoremH and a higher dimensional generalization of Lemma 2.1 are proved in Sections 4 and 5, respectively. The intermediate Section 3 is devoted to discussing the role of the computer in chaos detection.

Results on symbolic dynamics and various types of the pendulum equation can be found in a large number of papers. Two early results into this direction concern the standard pendulum equation with damping and variable length (but without an outer forcing term) $\ddot{x} + b\dot{x} + (1 + c \sin(\mu t)) \sin(x) = 0$. They were achieved by applying Melnikov’s approach [42] and a computer-assisted version of the shooting method [19], respectively. The concept of a chaotic oscillation for case $b = 0$ was defined in [14].

From the enormous (and still mathematically sound) literature on chaos in electrical circuits, we refer to the computer-assisted proofs of Galias [15] for chaos in Chua’s circuit as well as to the computer-assisted proof of Yang and Li [41] for chaos in Josephson junctions.

Chaos results for the time-periodic nonlinear Hill equation $\ddot{x} + q(t)g(x) = 0$ were obtained by topological and variational methods. The slightly more general time-periodic equations $\ddot{x} + b\dot{x} + q(t)g(x) = 0$ and $\ddot{x} + \partial W(t, x)/\partial x = h(t)$ were investigated in [7] and [6], respectively. For details, generalizations, and more references, see the forthcoming survey by Papini and Zanolin [30]. Note that Hubbard’s pendulum equation (1.1) is not captured by theoretical and computational results we are aware of.

2. Transition graph and chaos associated. For $j \in \mathbb{Z}$, define

$$\begin{aligned} Q_j &= \{(x_1, x_2) \in \mathbb{R}^2 \mid 3j + 1 \leq x_1 \leq 3j + 2, 0 \leq x_2 \leq 1\}, \\ \lambda_j &= \{x \in Q_j \mid x_1 = 3j + 1\}, \quad \rho_j = \{x \in Q_j \mid x_1 = 3j + 2\}, \\ E_j &= \{(x_1, x_2) \in \mathbb{R}^2 \mid 3j + 1 \leq x_1 \leq 3j + 2, |2x_2 - 1| > 1\}. \end{aligned}$$

Set $X = \cup_{j \in \mathbb{Z}} Q_j \subset \mathbb{R}^2$ and consider a continuous mapping $\varphi : X \rightarrow \mathbb{R}^2$ with coordinate functions φ_1, φ_2 . The *transition graph* $\mathcal{G}(\varphi)$ of φ is defined as a directed

graph with vertex set $\mathbf{V}(\mathcal{G}) = \mathbb{Z}$. For $j, \tilde{j} \in \mathbf{V}(\mathcal{G})$, the pair (j, \tilde{j}) belongs to the edge set $\mathbf{E}(\mathcal{G})$ of $\mathcal{G}(\varphi)$ if

$$(2.1) \quad \varphi(Q_j) \subset \mathbb{R}^2 \setminus \text{cl}(E_{\tilde{j}})$$

and the following alternative holds true:

either

$$(2.2) \quad \varphi_1(x) < 3\tilde{j} + 1 \text{ for } x \in \lambda_j \quad \text{and} \quad \varphi_1(x) > 3\tilde{j} + 2 \text{ for } x \in \rho_j$$

or

$$(2.3) \quad \varphi_1(x) > 3\tilde{j} + 2 \text{ for } x \in \lambda_j \quad \text{and} \quad \varphi_1(x) < 3\tilde{j} + 1 \text{ for } x \in \rho_j.$$

We write $\mathbf{V} = \mathbf{V}(\mathcal{G})$ and $\mathbf{E} = \mathbf{E}(\mathcal{G})$ in the sequel. For $N \in \mathbb{N}$, the directed graph $\mathcal{C} = \mathcal{C}(j_0, j_1, \dots, j_N)$ is a *directed $(N+1)$ -circle* in $\mathcal{G}(\varphi)$ if $\mathbf{V}(\mathcal{C}) = (j_0, j_1, \dots, j_N) \in \mathbf{V}^{N+1}$ and, with the convention $j_{N+1} = j_0$, $\mathbf{E}(\mathcal{C}) = \{(j_k, j_{k+1})\}_{k=0}^N \subset \mathbf{E}$. The directed graph $\mathcal{P} = \mathcal{P}(\{j_k\}_{k \in \mathbb{Z}})$ is a *directed biinfinite path* in $\mathcal{G}(\varphi)$ if $\mathbf{V}(\mathcal{P}) = \{j_k\}_{k \in \mathbb{Z}} \in \mathbf{V}^{\mathbb{Z}}$ and $\mathbf{E}(\mathcal{P}) = \{(j_k, j_{k+1})\}_{k \in \mathbb{Z}} \subset \mathbf{E}$. The definition of directed finite and infinite paths (i.e., paths having a root vertex) in $\mathcal{G}(\varphi)$ follows a similar pattern and is omitted.

LEMMA 2.1. *Let $\mathcal{C} = \mathcal{C}(j_0, j_1, \dots, j_N)$ be a directed circle in the transition graph $\mathcal{G}(\varphi)$. Then there is a finite sequence of points $\{q_k\}_{k=0}^N \subset X$ such that, with the convention $q_{N+1} = q_0$,*

$$q_{k+1} = \varphi(q_k) \quad \text{and} \quad q_k \in Q_{j_k}, \quad k = 0, 1, \dots, N.$$

Lemma 2.1 goes back to Mischaikow and Mrozek [25]. As stated above, it is a version of the main result in Zgliczynski [45]. The proof of (a higher-dimensional generalization of) Lemma 2.1 is postponed to Section 5.

COROLLARY 2.2. *Let $\mathcal{P} = \mathcal{P}(\{j_k\}_{k \in \mathbb{Z}})$ be a directed biinfinite path in the transition graph $\mathcal{G}(\varphi)$. Assume that either*

(A) *every directed infinite path in \mathcal{P} has infinitely many different vertices*

or

(B) *\mathcal{G} (as a directed graph) is connected.*

Then there is a biinfinite sequence of points $\{q_k\}_{k \in \mathbb{Z}} \subset X$ with the property that

$$q_{k+1} = \varphi(q_k) \quad \text{and} \quad q_k \in Q_{j_k}, \quad k \in \mathbb{Z}.$$

Proof. Case (A). Fix a positive integer $\ell = L$ and consider the finite path with consecutive vertices $(j_{-L}, j_{-L+1}, \dots, j_L) \in \mathbf{V}^{2L+1}$. Fix an integer $M > L$ so that $j_M \neq j_k$ for $k = -L, \dots, L$. Redefining φ on Q_{j_M} , we may assume that $(j_M, j_{-L}) \in \mathbf{E}$. Thus the extended finite sequence $(j_{-L}, \dots, j_L, j_{L+1}, \dots, j_M) \in \mathbf{V}^{L+1+M}$ forms the set of consecutive vertices of a directed circle in $\mathcal{G}(\varphi)$. Applying Lemma 2.1, we conclude there exists a finite sequence of points $\{q_k^L\}_{|k| \leq L} \subset X$ such that

$$q_{k+1}^L = \varphi(q_k^L) \text{ for } k = -L, \dots, L-1 \quad \text{and} \quad q_k^L \in Q_{j_k} \text{ for } k = -L, \dots, L.$$

Repeating the previous considerations for $\ell = L+1, L+2, \dots$, a standard Bolzano-Weierstrass subsequence argument in the limiting process $\ell \rightarrow \infty$ leads to the desired result.

Case (B). The connectedness of \mathcal{G} is equivalent to the property that every directed finite path in \mathcal{P} is contained in a directed circle of $\mathcal{G}(\varphi)$. Consequently, with easy modifications, the argument we applied in proving case (A) can be repeated.

□

Corollary 2.2 asserts the existence of a φ -trajectory visiting the Q_j 's in the prescribed order: A directed biinfinite path of type (A) or (B) of the transition graph is shadowed by a φ -trajectory. Directed $(N + 1)$ -circles in $\mathcal{G}(\varphi)$ are shadowed by $(N + 1)$ -periodic φ -trajectories. This is the content of Lemma 2.1.

Remark 1. If $N = 0$, then Lemma 2.1 simplifies to the Colorado fixed point theorem in [3]. If the vertical coordinate is missing, then Lemma 2.1 simplifies to a well-known result in one-dimensional dynamics (see e.g. Lemma III.1.4 in [34]) whose proof is based solely on the intermediate value theorem. The proof of a higher dimensional generalization of Lemma 2.1 in Section 5 mimics the standard derivation of Miranda theorem from Brouwer's fixed point theorem [31]. Note that Miranda theorem is nothing else but the higher dimensional counterpart of the intermediate value theorem. It is known to be equivalent to Brouwer's fixed point theorem and to many other important results in topology [44]. Its history goes back to as early as to Poincaré and Bohl. Recently, Miranda theorem has appeared as a root test in numerical analysis and interval computation [13], [12], [36] as well as in chaos theory for two-dimensional mappings [29], [4].

Remark 2. Observe that Lemma 2.1 remains valid if the right-hand side of inclusion (2.1) is weakened to $\mathbb{R}^2 \setminus E_j$ and the strict inequalities in (2.2) and (2.3) are replaced by their nonstrict counterparts. (In fact, for $\ell = 1, 2, \dots$, it is elementary to construct a modified map $\varphi^\ell : X \rightarrow \mathbb{R}^2$ satisfying $|\varphi^\ell - \varphi| < 1/\ell$ for which Lemma 2.1 (as stated above) applies. By passing $\ell \rightarrow \infty$, existence of the desired φ -periodic trajectory follows from the Bolzano-Weierstrass argument.) The reason of stating Lemma 2.1 in the form as presented above is to make the result stable with respect to small perturbations. Actually, if the conditions of Lemma 2.1 are met, and a continuous mapping $\tilde{\varphi} : \cup_{j \in \mathbb{Z}} Q_j \rightarrow \mathbb{R}^2$ satisfies $\max\{|\varphi(q) - \tilde{\varphi}(q)| \mid q \in \cup_{k=0}^N Q_{j_k}\} \leq \eta$ with η sufficiently small, then the $(N + 1)$ -tuple $(j_0, j_1, \dots, j_N) \in \mathbb{Z}^{N+1}$ forms a directed circle in $\mathcal{G}(\tilde{\varphi})$ as well. As we shall see in the sequel, it is exactly this robustness property of the transition graph which makes Lemma 2.1 applicable in computer-assisted proofs for horseshoe-type chaos. Stability with respect to small perturbations paves the way to stability with respect to numerical approximations including those with rounding errors.

Now we return to equation (1.1) investigated by Hubbard [20].

In what follows we point out how Corollary 2.2 applies and leads to a complete proof of Theorem 1.1. The strategy is to find a biinfinite sequence of pairwise disjoint compacta $\{K_j\}_{j \in \mathbb{Z}}$ in the Poincaré plane $\{(x, \dot{x}) \in \mathbb{R}^2\}$ such that, up to a coordinate transformation h , Corollary 2.2 applies to the associated Poincaré mapping $\Pi : (x(0), \dot{x}(0)) \rightarrow (x(2\pi), \dot{x}(2\pi))$ of equation (1.1). We need such a homeomorphism h of the Poincaré plane onto the standard plane $\{(x_1, x_2) \in \mathbb{R}^2\}$ that, for

$$\varphi = h\Pi h^{-1}|_X : X \rightarrow \mathbb{R}^2 \quad \text{with} \quad Q_j = h(K_j), \quad j \in \mathbb{Z},$$

Corollary 2.2 directly applies. Here, of course, $X = \cup_{j \in \mathbb{Z}} Q_j$ and $h\Pi h^{-1}|_X$ means the restriction of $h\Pi h^{-1}$ to X . Since Π is 2π -periodic with respect to the x variable and the number of different ε_k 's is three, the biinfinite sequence $\{K_j\}_{j \in \mathbb{Z}}$ is sought as a collection of the horizontal $2\ell\pi$ -translates of the three distinguished quadrangles L_0, M_0, R_0 with (compare to the notation in (1.3) and have a look at Figure 2.1)

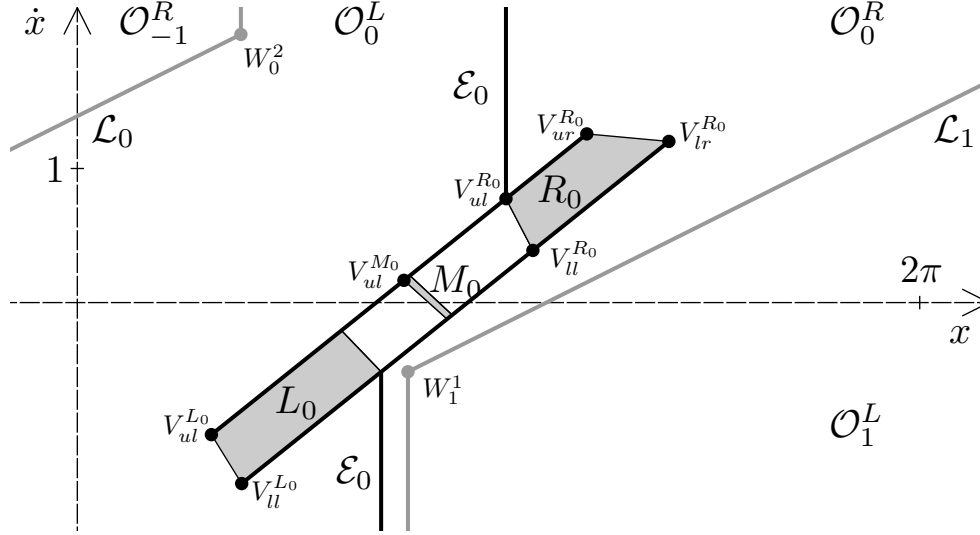


FIG. 2.1. Notation used in proving Theorem 1.1

$$K_{3\ell} = L_0 + (2\ell\pi, 0), \quad K_{3\ell+1} = M_0 + (2\ell\pi, 0), \quad K_{3\ell+2} = R_0 + (2\ell\pi, 0), \quad \ell \in \mathbb{Z}.$$

Given a biinfinite sequence $\{\varepsilon_k\}_{k \in \mathbb{Z}} \in \{-1; 0; 1\}^{\mathbb{Z}}$, it is crucial that the directed biinfinite path $\mathcal{P} = \mathcal{P}(\{j_k\}_{k \in \mathbb{Z}})$ with $j_k = 3\sigma_k + 1 + \varepsilon_k$ (where—as defined in Theorem 1.1— $\sigma_0 = 0$ and $\sigma_{k+1} = \sigma_k + \varepsilon_k$ for $k \in \mathbb{Z}$) is a subgraph of $\mathcal{G}(\varphi)$. Applying Corollary 2.2, trajectories satisfying (1.2) correspond to the directed biinfinite path $\mathcal{P} = \mathcal{P}(\{j_k\}_{k \in \mathbb{Z}})$ and vice versa.

Proof. [Proof of Theorem 1.1.] The successful realization of the strategy outlined above depends on the careful choice of the distinguished quadrangles L_0, M_0, R_0 and of the coordinate transformation h . In line with the horizontal 2π -translation invariance property of the collection $\{K_j\}_{j \in \mathbb{Z}}$, the continuous mapping $\varphi = h\Pi h^{-1}|_X$ is prescribed to be 9-periodic with respect to the x_1 variable. This can be guaranteed by requiring that the coordinate functions of homeomorphism $h : \{(x, \dot{x}) \in \mathbb{R}^2\} \rightarrow \{(x_1, x_2) \in \mathbb{R}^2\}$ satisfy

$$(2.4) \quad h_1(x + 2\pi, \dot{x}) = 9 + h_1(x, \dot{x}) \quad \text{and} \quad h_2(x + 2\pi, \dot{x}) = h_2(x, \dot{x}).$$

The existence of quadrangles L_0, M_0, R_0 that lead to a *transition graph suitably complicated* depends on the inner structure of the Poincaré mapping. Being far away from perturbative regimes, this inner structure is hardly accessible to a purely analytic-theoretical approach but can be revealed by computer experimentation quite easily.

Following Hubbard [20], consider quadrangles $K_0 = L_0, K_1 = M_0, K_2 = R_0$ as

$$K_j = \text{conv}\{V_{ul}^{K_j}, V_{ur}^{K_j}, V_{ll}^{K_j}, V_{lr}^{K_j}\}, \quad j = 0, 1, 2,$$

the closed convex hulls of their respective upper left, upper right, lower left, lower right vertices. (Letters L, M, R themselves stand for left, middle, and right, respectively.) The coordinates of these vertices are

$$\begin{aligned} V_{ul}^{L_0} &= (1.000, -0.985) & V_{ur}^{L_0} &= (1.970, -0.208) \\ V_{ll}^{L_0} &= (1.226, -1.350) & V_{lr}^{L_0} &= (2.226, -0.516), \end{aligned}$$

$$\begin{aligned} V_{ul}^{M_0} &= (2.436, 0.166) & , & & V_{ur}^{M_0} &= (2.481, 0.201) \\ V_{ll}^{M_0} &= (2.758, -0.123) & , & & V_{lr}^{M_0} &= (2.796, -0.092), \end{aligned}$$

$$\begin{aligned} V_{ul}^{R_0} &= (3.197, 0.775) & , & & V_{ur}^{R_0} &= (3.800, 1.258) \\ V_{ll}^{R_0} &= (3.398, 0.389) & , & & V_{lr}^{R_0} &= (4.412, 1.202). \end{aligned}$$

See Figure 2.1. For details on how the individual vertices were found, see the third paragraph of Section 3 below.

Consider also the broken line in Figure 2.1

$$\mathcal{L}_1 = \{\text{the vertical half-line below } W_1^1\} \cup [W_1^1, W_1^2] \cup \{\text{the vertical half-line above } W_1^2\}$$

where

$$W_1^1 = (w_1^1, w_2^1) = V_{lr}^{L_0} + (0.2, 0) \quad , \quad W_1^2 = (w_1^2, w_2^2) = (7.5, 2)$$

and $[W_1^1, W_1^2]$ stays for the closed line segment between W_1^1 and W_1^2 . The open strip between \mathcal{L}_1 and the translated broken line $\mathcal{L}_0 = \mathcal{L}_1 + (-2\pi, 0)$ is denoted by \mathcal{S}_0 . With ‘conv’ abbreviating the closed convex hull of the points that follow, define

$$\begin{aligned} \mathcal{D}_0 &= \{\text{the vertical half-line below } V_{lr}^{L_0}\} \cup L_0 \cup \text{conv}\{V_{ur}^{L_0}, V_{ul}^{M_0}, V_{ll}^{M_0}, V_{lr}^{L_0}\} \\ &\cup M_0 \cup \text{conv}\{V_{ur}^{M_0}, V_{ul}^{R_0}, V_{ll}^{R_0}, V_{lr}^{M_0}\} \cup R_0 \cup \{\text{the vertical half-line above } V_{ul}^{R_0}\}. \end{aligned}$$

The open strips between \mathcal{D}_0 and \mathcal{L}_0 resp. \mathcal{L}_1 are denoted by \mathcal{O}_0^L resp. \mathcal{O}_0^R . The union of the right-hand side boundary of the strip \mathcal{O}_0^L and the left-hand side boundary of the strip \mathcal{O}_0^R is denoted by \mathcal{B}_0 . Finally, we set

$$\mathcal{E}_0 = \mathcal{B}_0 \setminus \{(V_{ul}^{L_0}, V_{ll}^{L_0}) \cup (V_{ur}^{R_0}, V_{lr}^{R_0})\}$$

where $(V_{ul}^{L_0}, V_{ll}^{L_0})$ stays for the open line segment connecting $V_{ul}^{L_0}$ and $V_{ll}^{L_0}$ etc. (The closed line segment connecting $V_{ul}^{L_0}$ and $V_{ll}^{L_0}$ is denoted by $[V_{ul}^{L_0}, V_{ll}^{L_0}]$ etc. Note that \mathcal{E}_0 is the union of ten closed line segments and two closed half-lines. See Figure 2.1 again.)

The crucial properties responsible for the edge structure of the transition graph are

$$(2.5) \quad \Pi(R_{-1}), \Pi(M_0), \Pi(L_1) \subset \mathcal{S}_0 \setminus \mathcal{E}_0,$$

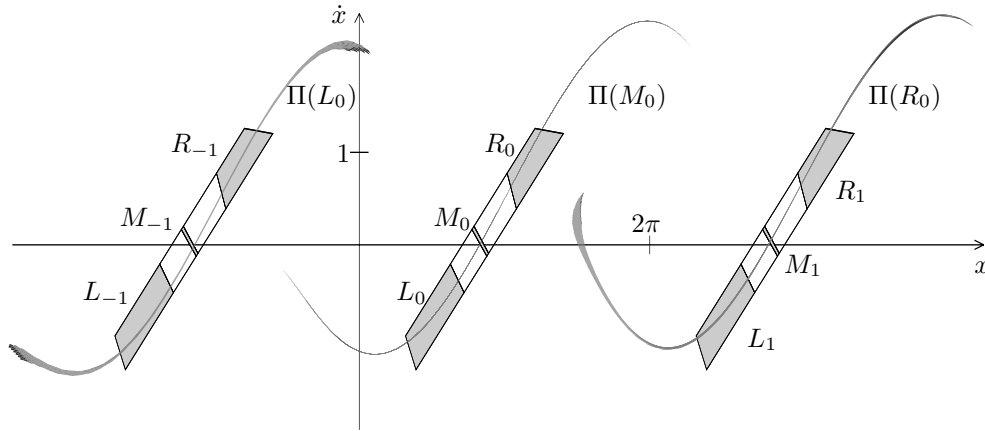
$$(2.6) \quad \Pi([V_{ul}^{R_{-1}}, V_{ll}^{R_{-1}}]), \Pi([V_{ul}^{M_0}, V_{ll}^{M_0}]), \Pi([V_{ur}^{L_1}, V_{lr}^{L_1}]) \subset \mathcal{O}_0^L,$$

$$(2.7) \quad \Pi([V_{ur}^{R_{-1}}, V_{lr}^{R_{-1}}]), \Pi([V_{ur}^{M_0}, V_{lr}^{M_0}]), \Pi([V_{ul}^{L_1}, V_{ll}^{L_1}]) \subset \mathcal{O}_0^R.$$

See Figure 2.2 portraying the sets $\Pi(L_0)$ (a translated copy of $\Pi(L_1)$) $\Pi(M_0)$, $\Pi(R_0)$ (a translated copy of $\Pi(R_{-1})$). The subset relations (2.5), (2.6), (2.7) are checked by computer. Note that the sets $\mathcal{S}_0 \setminus \mathcal{E}_0$, \mathcal{O}_0^L , \mathcal{O}_0^R are open and all the nine sets $\Pi(R_{-1})$, \dots , $\Pi([V_{ul}^{L_1}, V_{ll}^{L_1}])$ on the respective left-hand sides are compact. Hence inclusions (2.5), (2.6), (2.7) remain valid if the entire construction is repeated with the sets \mathcal{D}_0 , \mathcal{B}_0 , and \mathcal{E}_0 slightly thicker, i.e., if \mathcal{D}_0 , \mathcal{B}_0 , and \mathcal{E}_0 are replaced by their closed neighborhoods \mathcal{D} , \mathcal{B} , and \mathcal{E} suitably chosen.

Now we start with the construction of homeomorphism h subject to condition (2.4). We require also that $Q_j = h(K_j)$ with

$$\begin{aligned} (3j+1, 1) &= h(V_{ul}^{K_j}), \quad (3j+2, 1) = h(V_{ur}^{K_j}), \quad j = 0, 1, 2 \\ (3j+1, 0) &= h(V_{ll}^{K_j}), \quad (3j+2, 0) = h(V_{lr}^{K_j}), \quad j = 0, 1, 2 \end{aligned}$$

FIG. 2.2. Images of the distinguished quadrangles under Π

(i.e., the corresponding vertices are mapped to each other) and

$$(2.8) \quad \text{cl}(E_0 \cup E_1 \cup E_2) \subset h(\mathcal{E}) \quad , \quad \{(x_1, x_2) \in \mathbb{R}^2 \mid x_1 = 0\} = h(\mathcal{L}_0) .$$

Due to the piecewise linear boundaries of the sets involved, the construction of h is elementary. We have a great freedom in choosing h . Advanced results of two-dimensional topology are not needed. Note that, by translation symmetry, the broken line \mathcal{L}_1 is mapped onto the line of equation $x_1 = 9$.

Recall that $X = \cup_{j \in \mathbb{Z}} Q_j$. Property (2.5) and the inclusion in (2.8) imply that

$$\varphi(X) \subset \mathbb{R}^2 \setminus \text{cl}(\cup_{j \in \mathbb{Z}} E_j) .$$

Using (2.6), (2.7), we conclude that the transition graph of φ is as follows. The vertex set of $\mathcal{G}(\varphi)$ is obviously $\mathbf{V} = \mathbb{Z}$ and $\mathcal{G}(\varphi)$ is three-periodic in the sense that $(j, \tilde{j}) \in \mathbf{E}$ if and only if $(j + 3, \tilde{j} + 3) \in \mathbf{E}$. The edges starting from the vertex subset $\{0, 1, 2\}$ are as illustrated in Figure 2.3(a):

$$(0, -3); (0, -2); (0, -1); (1, 0); (1, 1); (1, 2); (2, 3); (2, 4); (2, 5) .$$

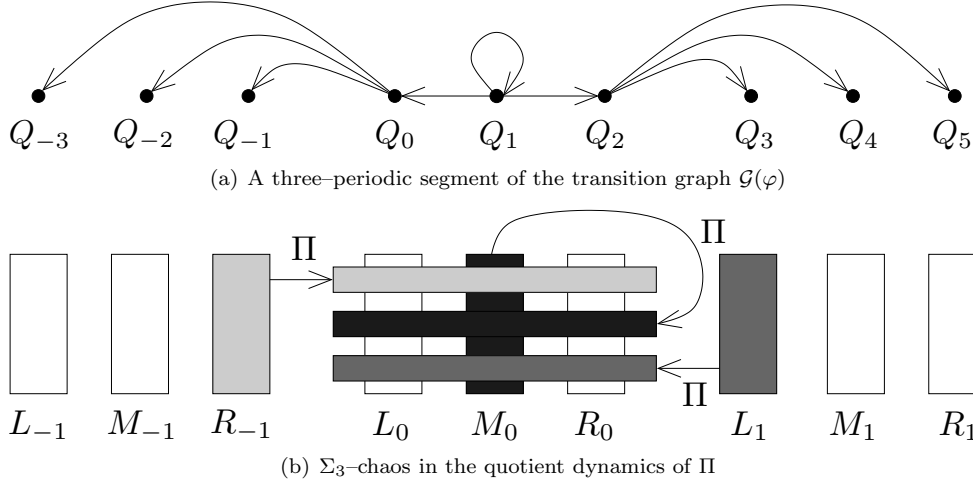
Thus we arrive at the schematic phase portrait of the Poincaré mapping presented in Figure 2.3(b).

Given a biinfinite sequence $\{\varepsilon_k\}_{k \in \mathbb{Z}} \in \{-1; 0; 1\}^{\mathbb{Z}}$, a quick analysis of the transition graph $\mathcal{G}(\varphi) = \mathcal{G}(h\Pi h^{-1}|X)$ shows that the directed biinfinite path $\mathcal{P} = \mathcal{P}(\{j_k\}_{k \in \mathbb{Z}})$ with $j_k = 3\sigma_k + 1 + \varepsilon_k$ (where—as defined in Theorem 1.1— $\sigma_0 = 0$ and $\sigma_{k+1} = \sigma_k + \varepsilon_k$ for $k \in \mathbb{Z}$) is a subgraph of $\mathcal{G}(\varphi)$. Trajectories satisfying (1.2) correspond to the directed biinfinite path $\mathcal{P} = \mathcal{P}(\{j_k\}_{k \in \mathbb{Z}})$ and vice versa.

This supplies all the details of proving Theorem 1.1: Corollary 2.2 applies and we are done. \square

The derivation of Theorem 1.1 follows the standard main argument in the Mischaikow-Mrozek framework for computer-assisted proofs. (Note that the invertibility of Π was not exploited but it will be needed for the backward invariance of the set Λ in Corollary 2.3 below). For the geometric background and details on the role of the computer, see Section 3.

It is an easy exercise to reformulate Theorem 1.1 in the language of symbolic dynamics [43], [34]. In fact, recall that $Q_j = h(K_j)$ and let $\Theta \subset X$ be the closure of


 FIG. 2.3. *Combinatorial complexity in Hubbard's forced damped pendulum equation*

all periodic points of φ that shadow the directed circles of $\mathcal{G}(\varphi)$. Set Θ is backward and forward invariant under φ . For $x \in \Theta$, formula

$$(c(x))_k = j_k \quad \text{whenever } \varphi^k(x) \in Q_{j_k} \quad \text{and } k \in \mathbb{Z},$$

defines a continuous itinerary mapping $c : \Theta \rightarrow \mathbb{Z}^{\mathbb{Z}}$. The inverse of homeomorphism h lifts everything to the Poincaré plane. Clearly $\Lambda = h^{-1}(\Theta)$ is backward and forward invariant under the Poincaré mapping Π and, for $\lambda = (x, \dot{x}) \in \Lambda$ with $d(\lambda) = c(h(\lambda))$,

$$(d(\lambda))_k = j_k \quad \text{whenever } \Pi^k(\lambda) \in K_{j_k}, \quad k \in \mathbb{Z}.$$

With S denoting the shift operator on $\mathbb{Z}^{\mathbb{Z}}$, we conclude that

$$c(\varphi(x)) = Sc(x) \quad \text{for each } x \in \Theta \quad \text{and} \quad d(\Pi(\lambda)) = Sd(\lambda) \quad \text{for each } \lambda \in \Lambda.$$

The entire construction reflects the horizontal 2π -translation symmetry of Π . The respective quotient maps are continuous and satisfy

$$\bar{d}(\bar{\Pi}(\bar{\lambda})) = \bar{S}\bar{d}(\bar{\lambda}) \quad \text{for each } \bar{\lambda} \in \bar{\Lambda}.$$

The quotient transition graph $\mathcal{G}(\bar{\varphi})$ is the complete directed graph on three vertices and thus the modulo 3 itinerary map $\bar{d} : \bar{\Lambda} \rightarrow \{0, 1, 2\}^{\mathbb{Z}}$ is onto. For convenience, note that

$$(\bar{d}(\bar{\lambda}))_k = 1 + \varepsilon_k \quad \text{for } \bar{\lambda} \in \bar{\Lambda} = \Lambda \cap \{(x, \dot{x}) \in \mathbf{R}^2 \mid 0 < x < 2\pi\}, \quad k \in \mathbb{Z}.$$

The quotient results can be restated in a compact form as follows.

COROLLARY 2.3 (Continuation of Theorem 1.1). *The modulo 2π Poincaré mapping $\bar{\Pi}$ on $\bar{\Lambda}$ is semiconjugate to the shift operator \bar{S} on Σ_3 , the space of three symbols.*

Actually, as it is suggested by Hubbard [20], \bar{d} is plausibly one-to-one and thus $\bar{\Pi}|_{\bar{\Lambda}}$ and \bar{S} are conjugate. See Figure 2.2 again and compare it to Figures 2.3(a) and 2.3(b).

3. Chaos detection by computer. What the computer is used for in the Mischaikow-Mrozek framework of computer-assisted proofs for chaos is *to check certain subset relations* (like (2.5), (2.6), (2.7)) and above all, *to find the subset relations to be checked* – basically, to find such a collection of ‘rectangular’ subsets of the phase space (like L_0, M_0, R_0) that the associated transition graph has at least two different, but intersecting circles.

The successful collection of ‘rectangular’ subsets is usually the result of computer experimentation with human overhead. In principle, by using constrained satisfaction techniques of global optimization [33], this trial and error process can be entirely left to the computer [9]. If three quadrangles are sought for, the search domain of the optimization procedure is a subset of a 24-dimensional parameter space (8 dimension for each quadrangle according to the coordinate pairs of the four vertices. The search for a successful collection of the ‘forbidden sets’ $\mathcal{L}_0, \mathcal{L}_1$, and \mathcal{E}_0 requires the introduction of some additional parameters.) The smaller the search domain the better. However, a ‘small’ search domain corresponds to a ‘good’ initial guess which cannot be obtained but only from some *a priori* known theoretical or numerical results on the structure of the dynamics. Typical candidates for members of a successful collection are quadrangles sitting on the unstable manifold of a transversal homoclinic saddle. We feel it is not inappropriate here to call the attention of the reader to a forthcoming paper [5] of ours where, within a 17-dimensional parameter space, the full power of the optimization method [4] is exploited. The main result is that \mathcal{H}^k , the k -th iterate of Hénon’s mapping with the classical parameters $a = 1.4$ and $b = 0.3$ has an embedded copy of the Σ_2 dynamics if and only if $k = 2, k = 4$, or $k \geq 6$. This is guaranteed by Smale’s abstract theory of transversal homoclinic saddles only for $k \geq k_0$ sufficiently large. (By the way, to the best of our knowledge, all existence proofs (e.g. [26], [11], [16]) for a transversal homoclinic saddle in the dynamics of \mathcal{H} are, in some way or the other, computer-assisted.)

In proving Theorem 1.1, the vertices of the distinguished quadrangles L_0, M_0, R_0 (as well as of the ‘forbidden sets’ $\mathcal{L}_0, \mathcal{L}_1, \mathcal{E}_0$) were chosen as indicated in Hubbard [20]. Though the coordinates of the individual vertices were not given explicitly by him, it was easy to adjust them on the basis of Figure 10 of his paper. This adjustment was made by hand and the optimization method [9] avoided. (Actually, what Hubbard works with are only three large quadrangles, the convex hulls of what we define as the sets $L_\ell \cup M_\ell \cup R_\ell$, $\ell = -1, 0, 1$ (and the ‘forbidden sets’ are not mentioned by him at all). At the first sight, it is plausible that the twelve vertices $V_{ul}^{L_0}, \dots, V_{lr}^{R_0}$ lie on the circumference of Hubbard’s large quadrangle. However, we could not establish such an arrangement. This seems to point to the differences between nonrigorous and rigorous computation.) Just like Hénon’s mapping \mathcal{H} , also the Poincaré mapping Π of Hubbard’s pendulum equation (1.1) has a homoclinic saddle. This saddle point is

$$P = (2.634\dots, 0.026\dots) \quad \text{with eigenvalues} \quad \mu_1 = 321.836\dots \quad \text{and} \quad \mu_2 = 0.001\dots$$

(all computations are rigorous). Of course P represents an unstable 2π -periodic solution which has bifurcated from the upward/top equilibrium position $x = \pi, \dot{x} = 0$ of the damped unforced pendulum. (Equation (1.1) has a second, asymptotically stable 2π -periodic solution which corresponds to the sink $Q = (4.236\dots, 0.392\dots)$ of the Poincaré mapping with eigenvalues $\mu_{1,2} = -0.725\dots \pm i 0.129\dots$ and which has bifurcated from the bottom equilibrium position $x = 0, \dot{x} = 0$ of the damped unforced pendulum. A computer-assisted argumentation shows there are no further 2π -periodic solutions.) Note that P is contained in M_0 and, one after the other, its

unstable manifold intersects the distinguished quadrangles in the rather strange order of $R_{-1}, M_{-1}, L_{-1}, L_0, M_0, R_0, L_1, M_0, R_1$.

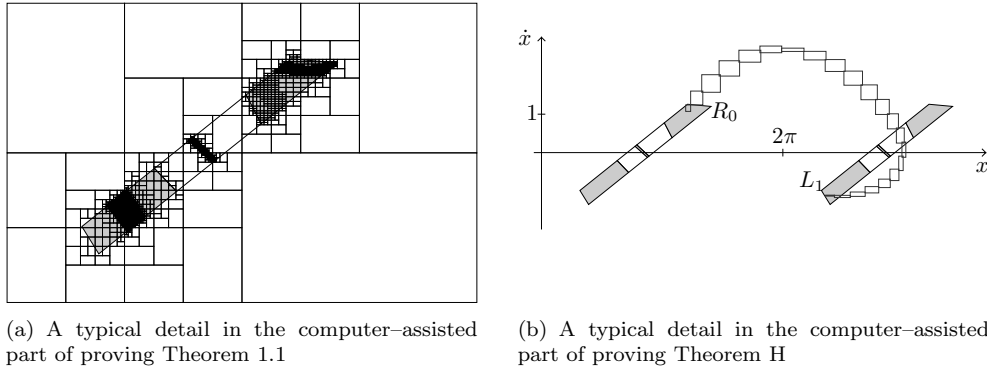
Unstable and stable manifolds of P intersect each other outside P . Apparently, this is a transversal intersection. We did not verify transversality by rigorous computation. The reason is that transversality alone, though guaranteeing the existence of a topological horseshoe, contains less information on the dynamics than a transition graph with carefully chosen ‘rectangular’ subsets. The next logical step forward should be rather the verification of the Conley-Moser invariant cone field conditions [43] leading (if it is really the case) to transversality as well as to the conjugacy between $\bar{\Pi}|\bar{\Lambda}$ and \bar{S} . Unfortunately, *the verification of inclusions (2.5), (2.6), (2.7) takes almost an entire hour on a personal computer of medium size*. See Figure 4.1(a). Consequently, we think there is little hope to check the invariant cone field conditions in a reasonable amount of time. Nevertheless, the semiconjugacy of $\bar{\Pi}|\bar{\Lambda}$ to \bar{S} established in Corollary 2.3 is not much worse than the conjugacy expected. Semiconjugacy to \bar{S} means that the dynamics is at least as complicated as the one of the shift operator on the space of three symbols whereas conjugacy would mean that the dynamics of $\bar{\Pi}|\bar{\Lambda}$ is exactly as complicated as the one of \bar{S} . What is easy to show is that $m(\bar{\Lambda})$, the Lebesgue measure of $\bar{\Lambda}$, equals zero. (This is clear because $\bar{\Pi}(\mathcal{C}) \subset \mathcal{C}$ for $\mathcal{C} = \{(x, \dot{x}) \in \mathbb{R}^2 \mid 0 \leq x < 2\pi, |\dot{x}| \leq 12\}$, $\bar{\Lambda} \subset \bigcap_{k=0}^{\infty} \bar{\Pi}^k(\mathcal{C})$, and $\bar{\Pi}$ contracts areas by a factor of $e^{-\pi/5}$, due to the damping and Liouville theorem [20].) Questions on further characteristics of chaos in Hubbard’s pendulum equation (1.1), e.g., the Wada property experimentally observed by Hubbard [20] or fine ergodic properties like the existence of a unique SRB measure (established for the Lorenz equation by Tucker [40]) and mixing (established for the Lorenz equation by Luzzato, Melbourne, and Paccout [24]) remain open.

Concluding this section, we note that the existence of a transition graph with two different but intersecting circles is implicit in an interesting paper by Stoffer and Palmer [38] on shadowing. Essentially, they prove that the existence of two hyperbolic periodic orbits that come sufficiently near to each other without remaining too close in the long run (e.g. whose minimal periods are highly nonresonant) implies the existence of an embedded horseshoe. This corresponds to the Levinson phenomenon that motivated Smale to construct the geometric horseshoe [37]. For related differences and similarities between the shadowing and the topological approach in computer-assisted proofs for chaos, see the recent paper of Coomes, Kocak, and Palmer [8].

4. Chaos in natural terms of the dynamics. The one-to-one correspondence between a set of the solutions to Hubbard’s pendulum equation (1.1) and the set of all biinfinite sequences on three symbols manifests itself in natural terms of the dynamics.

Looking at the pendulum, the distinguished quadrangles L_0, M_0, R_0 remain hidden, even to the most careful spectator. What he can easily notice, are high speed or low speed, the number of consecutive clockwise or counterclockwise returns, changes in the direction of swing and/or rotation, passages across the upper and/or the lower vertical position etc. In systematizing an abundance of different dynamical behaviour, the mind has a natural tendency to consider the consecutive occurrences of alternative, easily discernible events like heads-or-tails sequences in coin-tossing.

Theorems H and 1.1 have to be interpreted from this view-point. Any possible order of the mutually exclusive alternatives can be realized. Both observations describe the same combinatorial aspect of Σ_3 -chaos, the existence of ‘coin-tossing’ (coins with three sides) label sequences [22] for itineraries. However, the alternatives in Theorem 1.1 can hardly be observed whereas the alternatives in Theorem H are

FIG. 4.1. *Checking inclusions by interval computation*

quite transparent: There exist uncountably many solutions of Hubbard’s pendulum equation that can be distinguished from each other on the basis of their combinatorially different qualitative behaviour. This is what we might call combinatorial chaos in natural terms of the dynamics. Previous examples include symbolic dynamics in terms of consecutive return times in Alekseev’s three-body system [2], [20]; in terms of consecutive maxima and minima in the Lorenz systems [18]; in terms of the number of sign changes in consecutive time intervals of equal length [7], [39]; in terms of multibumps in bursting oscillations [35]; etc. Their natural place to occur is the vicinity of bifurcating homoclinic/heteroclinic orbit connections.

Proof. [Proof of Theorem H.] The derivation of from Theorem 1.1 requires investigating of what the solution map $(x(0), \dot{x}(0)) \rightarrow (x(t), \dot{x}(t))$ does between the Poincaré sections at $t_0 = 0$ and $t_1 = 2\pi$.

Consider the collection of motions of the forced damped pendulum with initial position $(x(0), \dot{x}(0)) \in R_0$ and final position $(x(2\pi), \dot{x}(2\pi)) \in L_1 \cup M_1 \cup R_1$. It is not hard to check by rigorous/interval computation that $0 < x(t) < 4\pi$ whenever $0 \leq t \leq 2\pi$ and

$$\{(x(t), \dot{x}(t)) \in \mathbb{R}^2 \mid 0 \leq t \leq 2\pi\} \cap \{(x, \dot{x}) \in \mathbb{R}^2 \mid x = 2\pi \text{ and } \dot{x} \leq 0\} = \emptyset.$$

In view of the intermediate value theorem, it follows that $x(t^*) = 2\pi$ for some $t^* \in (0, 2\pi)$, $x(t) \in (0, 2\pi)$ for $t \in [0, t^*)$, and $x(t) \in (2\pi, 4\pi)$ for $t \in (t^*, 2\pi]$. In other words, during the time interval $(0, 2\pi)$, the pendulum crosses the bottom position exactly once counterclockwise and does not point downwards at the time instants $t_0 = 0$ and $t_1 = 2\pi$. This holds true for all motions of the pendulum with initial position $(x(0), \dot{x}(0)) \in R_0$ and final position $(x(2\pi), \dot{x}(2\pi)) \in L_1 \cup M_1 \cup R_1$ (but not for all motions with initial position $(x(0), \dot{x}(0)) \in R_0$). In particular, this holds true for all distinguished $\sigma_0 = 0$, $\varepsilon_0 = 1$ (and, a fortiori, $\sigma_1 = 1$, $\varepsilon_1 \in \{-1, 0, 1\}$) motions of the pendulum captured by Theorem 1.1. Parts of the necessary computations in subcase $\sigma_0 = 0$, $\varepsilon_0 = 1$, $\sigma_1 = 1$, $\varepsilon_1 = -1$ are illustrated in Figure 4.1(b).

The remaining cases $\sigma_0 = 0$, $\varepsilon_0 = 0$ and $\sigma_0 = 0$, $\varepsilon_0 = -1$ cases were settled similarly. *The total computing time was less than two minutes on an average personal computer.* \square

The relation between symbolic dynamics and oscillation patterns is worth of further investigation. We ask if symbolic dynamics appears in terms of crossing the bottom *and the top* equilibrium position.

5. Lemma 2.1 in higher dimension. A simple proof. Let m, n be fixed nonnegative integers, and let $\mathbf{V} \subset \mathbb{Z}$ be a finite or countably infinite indexing set. Boundary and interior of a compact set S in a Euclidean space \mathbb{R}^k is denoted by ∂S and $\text{int}(S)$, respectively. The closed neighborhood of radius $R > 0$ of a point p and a set S in \mathbb{R}^k is denoted by $\mathcal{B}^k[p, R]$ and $\mathcal{B}^k[S, R]$, respectively. Norm and scalar product in \mathbb{R}^k are denoted by $\|\cdot\|$ and $\langle \cdot, \cdot \rangle$.

Consider the collection of the rectangular sets of the form

$$Q_j = \{x = (u, s) \in \mathbb{R}^m \times \mathbb{R}^n \mid u \in U_j, s \in S_j\}, \quad j \in \mathbf{V}$$

where $\{U_j\}_{j \in \mathbf{V}}$ and $\{S_j\}_{j \in \mathbf{V}}$ are compact topological balls in \mathbb{R}^m and in \mathbb{R}^n , respectively. Note that S_j is a retract of \mathbb{R}^n . Let $r_j : \mathbb{R}^n \rightarrow S_j$ be a retraction, $j \in \mathbf{V}$.

Let $X = \cup_{j \in \mathbf{V}} Q_j \subset \mathbb{R}^m \times \mathbb{R}^n$ and consider a continuous mapping $\varphi : X \rightarrow \mathbb{R}^m \times \mathbb{R}^n$ with coordinate functions φ_u, φ_s . It is assumed that $Q_j \cap Q_k = \emptyset$ for $j \neq k$ and that $\{j \in \mathbf{V} \mid Q_j \cap \{(u, s) \in \mathbb{R}^m \times \mathbb{R}^n \mid \|u\| + \|s\| < R\} \neq \emptyset\}$ is finite for any $R > 0$.

The *transition graph* $\mathcal{G}(\varphi)$ of φ is defined as a directed graph with vertex set \mathbf{V} . For $j, \tilde{j} \in \mathbf{V}$, the pair (j, \tilde{j}) belongs to the edge set \mathbf{E} of $\mathcal{G}(\varphi)$ if

$$(5.1) \quad \varphi(Q_j) \subset \mathbb{R}^m \times \mathbb{R}^n \setminus U_{\tilde{j}} \times (\mathbb{R}^n \setminus S_{\tilde{j}})$$

and there exist positive constants $\eta_0 = \eta_0(j, \tilde{j})$ and $\kappa_0 = \kappa_0(j, \tilde{j})$ such that one of the following two conditions is satisfied:

either

$$(5.2) \quad \begin{aligned} v_j + \kappa(u_{\tilde{j}} - \varphi_u(v_j, s_j)) \in U_{\tilde{j}} \quad \text{whenever} \\ v_j \in U_j, d(v_j, \partial U_j) \leq \eta_0, s_j \in S_j, u_{\tilde{j}} \in U_{\tilde{j}} \quad \text{and} \quad 0 \leq \kappa \leq \kappa_0 \end{aligned}$$

or

$$(5.3) \quad \begin{aligned} v_j - \kappa(u_{\tilde{j}} - \varphi_u(v_j, s_j)) \in U_{\tilde{j}} \quad \text{whenever} \\ v_j \in U_j, d(v_j, \partial U_j) \leq \eta_0, s_j \in S_j, u_{\tilde{j}} \in U_{\tilde{j}} \quad \text{and} \quad 0 \leq \kappa \leq \kappa_0. \end{aligned}$$

The definition of the transition graph in Section 2 is more restrictive. If $m = n = 1$, then condition (5.1) is equivalent to $\varphi(Q_j) \subset \mathbb{R}^2 \setminus E_{\tilde{j}}$, a weakening of condition (2.1) discussed in Remark 2. Similarly, with $\eta_0 = 1 - \vartheta_0$ and κ_0 suitably chosen (it is enough to take both $\vartheta_0 > 0$ and $\kappa_0 = \kappa_0(\vartheta_0) > 0$ sufficiently small), conditions (5.2) and (5.3) are implied by conditions (2.2) and (2.3), respectively.

With the notion of the transition graph redefined in $\mathbb{R}^m \times \mathbb{R}^n$, $m, n \geq 1$, the text of Lemma 2.1 in higher dimension coincides with that of the original Lemma 2.1 word for word. Now we pass to the proof of this generalization. Conditions (5.2) and (5.3) will be illuminated and analyzed thereafter.

Proof. [Proof of Lemma 2.1 in $\mathbb{R}^m \times \mathbb{R}^n$.] The strategy is to rewrite the system of equations

$$x_{k+1} = \varphi(x_k) \quad \text{and} \quad x_k \in Q_{j_k}, \quad k = 0, 1, \dots, N$$

as a fixed point equation $(x_0, x_1, \dots, x_N) = \mathcal{F}(x_0, x_1, \dots, x_N)$ in the product space $\prod_{k=0}^N Q_{j_k} \subset (\mathbb{R}^m \times \mathbb{R}^n)^{N+1}$ and to check that all conditions of Brouwer's fixed point theorem are satisfied.

Fix a positive constant

$$\kappa^* \leq \min_{k=0,1,\dots,N} \kappa_0(j_k, j_{k+1}) \quad \text{such that} \quad \kappa^* C^* \leq \min_{k=0,1,\dots,N} \eta_0(j_k, j_{k+1})$$

where

$$C^* = \max_{k=0,1,\dots,N} \max\{\|u_{k+1} - \varphi_u(x_k)\| \mid u_{k+1} \in U_{j_{k+1}}, x_k \in Q_{j_k}\}.$$

For $(x_0, x_1, \dots, x_N) \in \prod_{k=0}^N Q_{j_k}$, we set coordinatewise

$$(\mathcal{F}(x_0, x_1, \dots, x_N))_k = (u_k + \varepsilon_k \kappa^*(u_{k+1} - \varphi_u(x_k)), r_{j_k}(\varphi_s(x_{k-1}))) \in \mathbb{R}^m \times \mathbb{R}^n.$$

Here ε_k depends on the pair $(j, \tilde{j}) = (j_k, j_{k+1})$ by taking $\varepsilon_k = 1$ if condition (5.2) and $\varepsilon_k = -1$ if condition (5.3) is satisfied, $k = 0, 1, \dots, N$.

Since $x_{N+1} = x_0$, $x_{-1} = x_N$ by convention, we shift the indices in the \mathbb{R}^n -coordinate, and see that the fixed point equation $(x_0, x_1, \dots, x_N) = \mathcal{F}(x_0, x_1, \dots, x_N)$ in $\prod_{k=0}^N Q_{j_k}$ is equivalent to the system of equations

$$(5.4) \quad u_{k+1} = \varphi_u(x_k) \quad \text{and} \quad s_{k+1} = r_{j_{k+1}}(\varphi_s(x_k)) \quad , \quad k = 0, 1, \dots, N.$$

By using condition (5.1), $\varphi_s(x_k) \in S_{j_{k+1}}$. Hence $r_{j_{k+1}}(\varphi_s(x_k)) = \varphi_s(x_k)$, and system (5.4) simplifies to

$$u_{k+1} = \varphi_u(x_k) \quad \text{and} \quad s_{k+1} = \varphi_s(x_k) \quad , \quad i.e., \quad x_{k+1} = \varphi(x_k) \quad , \quad k = 0, 1, \dots, N.$$

It is clear that $\prod_{k=0}^N Q_{j_k}$ is a compact topological ball in $(\mathbb{R}^m \times \mathbb{R}^n)^{N+1}$ and $\mathcal{F} : \prod_{k=0}^N Q_{j_k} \rightarrow (\mathbb{R}^m \times \mathbb{R}^n)^{N+1}$ is a continuous function. It remains to prove that

$$(\mathcal{F}(x_0, x_1, \dots, x_N))_k \in Q_{j_k} \quad \text{whenever} \quad (x_0, x_1, \dots, x_N) \in \prod_{k=0}^N Q_{j_k} \quad ,$$

$k = 0, 1, \dots, N$. Since $r_{j_k}(\varphi_s(x_{k-1})) \in S_{j_k}$, we can pass to the \mathbb{R}^m -coordinate and have to check only that

$$(5.5) \quad u_k + \varepsilon_k \kappa^*(u_{k+1} - \varphi_u(x_k)) \in U_{j_k} \quad \text{if} \quad x_k = (u_k, s_k) \in Q_{j_k} \quad \text{and} \quad u_{k+1} \in U_{j_{k+1}}.$$

If $u_k \in U_{j_k}$ with $d(u_k, \partial U_{j_k}) \leq \eta_0(j_k, j_{k+1})$, then—depending on the value of ε_k —(5.5) reduces to (5.2) or (5.3) with $\kappa = \kappa^*$. On the other hand, if $u_k \in U_{j_k}$ with $d(u_k, \partial U_{j_k}) > \eta_0(j_k, j_{k+1})$, then (5.5) follows via inequality $\kappa^* \|u_{k+1} - \varphi_u(x_k)\| \leq \kappa^* C^* \leq \eta_0(j_k, j_{k+1})$, $k = 0, 1, \dots, N$. \square

Geometrically, both condition (5.2) and the alternative condition (5.3) mean that $U_{\tilde{j}}$ is ‘surrounded by’ $\varphi_u(\partial U_j \times S_j)$. In the special case $U_j = U_{\tilde{j}} = \mathcal{B}^m[0, 1]$ and $S_j = \mathcal{B}^n[0, 1]$ (compact unit balls in the respective Euclidean spaces), condition (5.2) is implied by inequality

$$\langle \varphi_u(u, s) - \tilde{u}, u \rangle > 1 \quad \text{whenever} \quad u, \tilde{u} \in \mathbb{R}^m, \quad s \in \mathbb{R}^n, \quad \|u\| = 1, \quad \|\tilde{u}\|, \|s\| \leq 1$$

resembling certain geometric conditions in various consequences of Brouwer’s fixed point theorem [44].

The rest of the paper is devoted to a technical analysis of conditions (5.2) and (5.3). By symmetry, this analysis reduces to investigating (5.2). Condition (5.2) will be replaced by the slightly stronger condition (5.6) which is stable with respect to small perturbations of φ_u including numerical approximations with rounding errors. A second advantage of (5.6) over (5.2) is that condition (5.6) can be checked more

easily. All in all, condition (5.6) fits better to computer-assisted proofs than (5.2). The paper ends with the somewhat more convenient and transparent condition (5.8).

PROPOSITION 5.1. *Condition (5.2) is a consequence of the following requirement. There exist positive constants $\lambda_0 = \lambda_0(j, \tilde{j})$ and $\Delta = \Delta(j, \tilde{j})$ such that*

$$(5.6) \quad \begin{aligned} & u_j + \lambda(w_{\tilde{j}} - \varphi_u(u_j, s_j)) \in U_j \quad \text{whenever} \\ & u_j \in \partial U_j, \quad s_j \in S_j, \quad w_{\tilde{j}} \in \mathcal{B}^m[U_{\tilde{j}}, \Delta] \quad \text{and} \quad 0 \leq \lambda \leq \lambda_0. \end{aligned}$$

Proof. We omit indices j, \tilde{j} in the sequel and write $U = U_j$, $S = S_j$, and $W = U_{\tilde{j}}$.

To the contrary, assume that condition (5.6) is satisfied but (5.2) is not. Then there are sequences $\{v_\ell\} \subset U$, $\{s_\ell\} \subset S$, $\{w_\ell\} \subset W$, $\{\kappa_\ell\} \subset \mathbb{R}^+$ with the properties that

$$(5.7) \quad p_\ell = v_\ell + \kappa_\ell(w_\ell - \varphi_u(v_\ell, s_\ell)) \notin U, \quad \text{for } \ell = 1, 2, \dots$$

and either $v_\ell \rightarrow \partial U$ or $\kappa_\ell \rightarrow 0$.

Suppose first that $\kappa_\ell \rightarrow 0$. Since $v_\ell \in U$ and $p_\ell \notin U$, there exists a $\kappa_\ell^* \in [0, \kappa_\ell)$ such that

$$z_\ell = v_\ell + \kappa_\ell^*(w_\ell - \varphi_u(v_\ell, s_\ell)) \in \partial U, \quad \text{for } \ell = 1, 2, \dots$$

Note that $0 < \kappa_\ell - \kappa_\ell^* \leq \lambda_0$ and $\|\varphi_u(z_\ell, s_\ell) - \varphi_u(v_\ell, s_\ell)\| \leq \Delta$ for ℓ large enough. In view of condition (5.6), we conclude that

$$p_\ell = z_\ell + (\kappa_\ell - \kappa_\ell^*)(w_\ell + \varphi_u(z_\ell, s_\ell) - \varphi_u(v_\ell, s_\ell)) - \varphi_u(z_\ell, s_\ell) \in U$$

for ℓ large enough, a contradiction to (5.7).

Suppose now that $v_\ell \rightarrow \partial U$. There is no loss of generality in assuming that $v_\ell \rightarrow v^*$ for some $v^* \in \partial U$, $s_\ell \rightarrow s^*$ for some $s^* \in S$, and $0 < \inf \kappa_\ell \leq \sup \kappa_\ell \leq \lambda_0$. In particular, $\|\frac{v_\ell - v^*}{\kappa_\ell} - \varphi_u(v_\ell, s_\ell) + \varphi_u(v^*, s^*)\| \leq \Delta$ for ℓ large enough. In view of condition (5.6), we conclude that

$$p_\ell = v^* + \kappa_\ell \left[\left(w_\ell + \frac{v_\ell - v^*}{\kappa_\ell} - \varphi_u(v_\ell, s_\ell) + \varphi_u(v^*, s^*) \right) - \varphi_u(v^*, s^*) \right] \in U$$

for ℓ large enough, a contradiction to (5.7). \square

PROPOSITION 5.2. *Condition (5.6) is a consequence of the following requirement. There exists a positive constant $\delta = \delta(j, \tilde{j})$ such that*

$$(5.8) \quad \begin{aligned} & u_j + \mu(w_{\tilde{j}} - \varphi_u(u_j, s_j)) \in \text{int}(U_j) \quad \text{whenever} \\ & u_j \in \partial U_j, \quad s_j \in S_j, \quad w_{\tilde{j}} \in \mathcal{B}^m[U_{\tilde{j}}, \delta] \quad \text{and} \quad 0 < \mu \leq \mu_0 \quad \text{with some } \mu_0 = \mu_0(u_j, s_j, w_{\tilde{j}}). \end{aligned}$$

Proof. As before, we write $U = U_j$, $S = S_j$, and $W = U_{\tilde{j}}$.

Fix $u^* \in \partial U$, $s^* \in S$ and $w^* \in W$. By compactness, it is enough to point out the existence of two positive constants $\tau = \tau(u^*, s^*, w^*)$ and $\lambda^* = \lambda^*(u^*, s^*, w^*, \tau)$ such that, given $u \in \partial U$, $s \in S$ and $w \in \mathcal{B}^m[W, \delta]$ with $\|u - u^*\| \leq \tau$, $\|s - s^*\| \leq \tau$, $\|w - w^*\| \leq \tau$, it holds true that

$$u + \lambda(w - \varphi_u(u, s)) \in U \quad \text{whenever } 0 \leq \lambda \leq \lambda^*.$$

By continuity, there is a $0 < \sigma < \delta$ such that, given $w \in \mathcal{B}^m[w^*, \sigma]$, $q \in U \cap \mathcal{B}^m[u^*, \sigma]$ arbitrarily,

$$(5.9) \quad \tilde{w} - \varphi_u(q, s^*) = w - \varphi_u(u^*, s^*) \quad \text{for some } \tilde{w} \in \mathcal{B}^m[w^*, \delta].$$

In view of condition (5.6) applied for (u^*, s^*, w^*) , we may assume that

$$u^* + \alpha_+^*(w^* - \varphi_u(u^*, s^*)) \in \text{int}(U) \cap \partial \mathcal{B}^m[u^*, \sigma] \quad \text{for some } \alpha_+^* > 0.$$

As a corollary, a simple geometric argument implies the existence of a constant $0 < \eta < \sigma$ with the properties as follows. Given $p \in \mathcal{B}^m[u^*, \eta]$ and $w \in \mathcal{B}^m[w^*, \eta]$ arbitrarily,

$$p + \alpha_+(w - \varphi_u(u^*, s^*)) \in \text{int}(U) \cap \partial \mathcal{B}^m[u^*, \sigma] \quad \text{for some } \alpha_+ = \alpha_+(p, w) > 0$$

where α_+ is unique, function $(p, w) \rightarrow \alpha_+(p, w)$ is continuous, and $\alpha_+(u^*, w^*) = \alpha_+^*$. For later use, we note that

$$\alpha_* = \inf\{\alpha_+(p, w) \mid p \in \mathcal{B}^m[u^*, \eta], w \in \mathcal{B}^m[w^*, \eta]\} > 0$$

by compactness. Similarly, observe there exists a constant $0 < \tau < \eta$ such that, given $w \in \mathcal{B}^m[w^*, \tau]$, $u \in U \cap \mathcal{B}^m[u^*, \tau]$, $s \in S \cap \mathcal{B}^m[s^*, \tau]$ arbitrarily,

$$(5.10) \quad \hat{w} - \varphi_u(u^*, s^*) = w - \varphi_u(u, s) \quad \text{for some } \hat{w} \in \mathcal{B}^m[w^*, \eta].$$

Consider now the straight line segment

$$L_{p,w} = \{p + \lambda(w - \varphi_u(u^*, s^*)) \mid \lambda \geq 0\} \cap \mathcal{B}^m[u^*, \sigma]$$

and assume that $q = p + \gamma_0(w - \varphi_u(u^*, s^*)) \in \partial U \cap L_{p,w}$ for some $\gamma_0 < \alpha_+$. By using property (5.9), condition (5.6) (when applied for (q, s^*, \tilde{w})) implies that

$$p + \gamma(w - \varphi_u(u^*, s^*)) = q + (\gamma - \gamma_0)(\tilde{w} - \varphi_u(q, s^*)) \in \text{int}(U)$$

for $\gamma > \gamma_0$, $|\gamma - \gamma_0|$ small. By an elementary connectedness argument in one dimension, we conclude that $L_{p,w} \cap U$ is a compact interval with an endpoint on $\partial \mathcal{B}^m[u^*, \sigma]$. If, in particular, $p = u \in \partial U \cap \mathcal{B}^m[u^*, \tau]$, $s \in S \cap \mathcal{B}^m[s^*, \tau]$ and $w \in \mathcal{B}^m[w^*, \tau]$, then

$$\{u + \lambda(w - \varphi_u(u, s)) \mid \lambda \geq 0\} \cap \mathcal{B}^m[u^*, \sigma] = L_{u,\hat{w}}$$

by property (5.10) and thus $u + \lambda(w - \varphi_u(u, s)) \in U$ for $0 \leq \lambda \leq \alpha_+(u, \hat{w})$. Hence $\lambda^* = \lambda^*(u^*, s^*, w^*)$ can be taken for $\alpha_* > 0$. \square

REFERENCES

- [1] G. ALEFELD, AND G. MAYER, *Interval analysis: Theory and applications*, J. Comput. Appl. Math., 121 (2000), pp. 421–464.
- [2] V.M. ALEXEEV, *On the capture orbits for the three-body problem for negative energy constant*, Uspekhi Mat. Nauk., 24 (1969), pp. 185–186.
- [3] K.T. ALLIGOOD, T.D. SAUER, AND J.A. YORKE, *Chaos. An Introduction to Dynamical Systems*, Springer, Berlin, 1997.
- [4] B. BÁNHÉLYI, T. CSENDES, AND B.M. GARAY, *Optimization and the Miranda approach in detecting horseshoe-type chaos by computer*, Int. J. Bifurc. Chaos, 17 (2007), pp. 735–747.
- [5] B. BÁNHÉLYI, T. CSENDES, AND B.M. GARAY, *Σ_2 -chaos for iterates of the classical Hénon mapping*, 2007, (in preparation) .

- [6] E. BOSETTO, AND E. SERRA, *A variational approach to chaotic dynamics in periodically forced nonlinear oscillators*, Ann. IHP Anal. Non Linéaire, 17 (2000), pp. 673–709.
- [7] A. CAPIETTO, W. DAMBROSIO, AND D. PAPINI, *Superlinear indefinite equations on the real line and chaotic dynamics*, J. Differ. Eq., 181 (2002), pp. 419–438.
- [8] B.A. COOMES, H. KOCAK, AND K.J. PALMER, *Homoclinic shadowing*, J. Dynam. Differ. Eq., 17 (2005), pp. 175–215.
- [9] T. CSENDES, B.M. GARAY, AND B. BÁNHÉLYI, *A verified optimization technique to locate chaotic regions of a Hénon system*, J. of Global Optimiz., 35 (2006), pp. 145–160.
- [10] M. DELLNITZ, AND O. JUNGE, *Set oriented numerical methods for dynamical systems*, in *Handbook of Dynamical Systems, Vol. 2*, (ed. by B. Fiedler), North-Holland, Amsterdam, 2002, pp. 221–264.
- [11] V. FRANCESCHINI, AND L. RUSSO, *Stable and unstable manifolds of the Hénon mapping*, J. Statist. Phys., 25 (1981), pp. 757–769.
- [12] A. FROMMER, AND B. LANG, *Existence tests for solutions of nonlinear equations using Borsuk’s theorem*, SIAM J. Numer. Anal., 43 (2005), pp. 1348–1361.
- [13] A. FROMMER, B. LANG, AND M. SCHNURR, *A comparison of the Moore and Miranda existence tests*, Computing, 72 (2004), pp. 349–354.
- [14] M. FURI, M. MARTELLI, M. O’NEIL, AND C. STAPLES, *Chaotic orbits of a pendulum with variable length*, Electron. J. Differ. Eq., No.36 (2004), pp. 14.
- [15] Z. GALIAS, *Positive topological entropy of Chua’s circuit: a computer-assisted proof*, Int. J. Bifurcations and Chaos, 7 (1997), pp. 331–349.
- [16] Z. GALIAS, AND P. ZGLICZYNSKI, *Abundance of homoclinic and heteroclinic orbits and rigorous bounds for the topological entropy for the Hénon map*, Nonlinearity, 14 (2001), pp. 909–932.
- [17] M. GIDEA, AND P. ZGLICZYNSKI, *Covering relations for multidimensional dynamical systems*, J. Differ. Eq., 202 (2004), pp. 32–58.
- [18] B. HASSARD, B. ZHANG, S.P. HASTINGS, AND W.C. TROY, *A computer proof that the Lorenz equations have “chaotic” solutions*, Appl. Math. Lett., 7 (1994), pp. 79–83.
- [19] S.P. HASTINGS, AND J.B. MCLEOD, *Chaotic motion of a pendulum with oscillatory forcing*, Amer. Math. Monthly, 100 (1993), pp. 563–572.
- [20] J.H. HUBBARD, *The forced damped pendulum: chaos, complication and control*, Amer. Math. Monthly, 106 (1999), pp. 741–758.
- [21] J.A. KENNEDY, S. KOCAK, AND J.A. YORKE, *A chaos lemma*, Amer. Math. Monthly, 108 (2001), pp. 411–423.
- [22] U. KIRCHGRABER, AND D. STOFFER, *On the definition of chaos*, Z. Angew. Math. Mech., 69 (1989), pp. 175–185.
- [23] R. KLATTE, U. KULISCH, A. WIETHOFF, C. LAWO, AND M. RAUCH, *C-XSC – A C++ Class Library for Extended Scientific Computing*, Springer, Berlin, 2003.
- [24] S. LUZZATTO, I. MELBOURNE, AND F. PACCAUT, *The Lorenz attractor is mixing*, J. Comm. Math. Phys., 260 (2005), pp. 393–401.
- [25] K. MISCHAIKOW, AND M. MROZEK, *Chaos in the Lorenz equations: a computer-assisted proof*, Bull. Amer. Math. Soc., 32 (1995), pp. 66–72.
- [26] M. MISIUREWICZ, AND B. SZEWC, *Existence of a homoclinic point for the Hénon mapping*, Comm. Math. Phys., 75 (1980), pp. 285–291.
- [27] N.S. NEDIALKOV, *VNODE – A validated solver for initial value problems for ordinary differential equations*, Available at www.cas.mcmaster.ca/~nedialk/Software/VNODE/VNODE.shtml, 2001.
- [28] N.S. NEDIALKOV, K.R. JACKSON, AND G.F. CORLISS, *Validated solutions of initial value problems for ordinary differential equations*, Appl. Math. Comput., 105 (1999), pp. 21–68.
- [29] D. PAPINI, AND F. ZANOLIN, *Fixed points, periodic points, and coin-tossing sequences for mappings defined on two-dimensional cells*, Fixed Point Theory and Appl., 2 (2004), pp. 113–134.
- [30] D. PAPINI, AND F. ZANOLIN, *Some results on periodic points and chaotic dynamics arising from the study of the nonlinear Hill equation*, Rend. Sem. Mat. Univ. Pol. Torino, 2007, (in print).
- [31] L.C. PICCININI, G. STAMPACCIA, AND G. VIDOSSICH, *Ordinary Differential Equations in \mathbb{R}^n* , Springer, Berlin, 1984.
- [32] M. PIREDDU, AND F. ZANOLIN, *Fixed points for dissipative-repulsive systems and topological dynamics of mappings defined on N-dimensional cells*, Advanced Nonlinear Studies, 5 (2005), pp. 411–440.
- [33] H. RATSCHKE, AND J. ROKNE, *New Computer Methods for Global Optimization*, Ellis Horwood, Chichester, 1988.
- [34] C. ROBINSON, *Dynamical Systems. Stability, Symbolic Dynamics, and Chaos*, RCR Press, Boca

- Raton, 1999.
- [35] J. RUBIN, AND D. TERMAN, [2002] *Geometric singular perturbation analysis of neuronal dynamics*, in *Handbook of Dynamical Systems vol. 2*, ed. Fiedler, B., North-Holland, Amsterdam, 2002, pp. 93–146.
 - [36] M. SCHNURR, *On the proofs of some statements concerning the theorems of Kantorovich, Moore and Miranda*, *Reliable Comp.*, 11 (2005), pp. 77–85.
 - [37] S. SMALE, *The Mathematics of Time*, Springer, Berlin, 1980.
 - [38] D. STOFFER, AND K.J. PALMER, *Rigorous verification of chaotic behaviour of maps using validated shadowing*, *Nonlinearity*, 12 (1999), pp. 1683–1689.
 - [39] S. TERRACINI, AND G. VERSINI, *Solutions of prescribed number of zeroes to a class of superlinear ODE's systems*, *NODEA Nonlin. Differ. Equat. Appl.*, 8 (2001), pp. 323–341.
 - [40] W. TUCKER, *A rigorous ODE solver and Smale's 14th problem*, *Found. Comput. Math.*, 2 (2002), pp. 53–117.
 - [41] X.S. YANG, AND Q. LI, *A computer-assisted proof of chaos in Josephson junctions*, *Chaos Solitons Fractals*, 27 (2006), pp. 25–30.
 - [42] S. WIGGINS, *On the detection and dynamical consequences of orbits homoclinic to hyperbolic periodic orbits and normally hyperbolic invariant tori in a class of ordinary differential equations*, *SIAM. J. Applied Math.*, 48 (1988), pp. 262–285.
 - [43] S. WIGGINS, *Introduction to Applied Nonlinear Dynamical Systems and Chaos*, Springer, Berlin, 2003.
 - [44] E. ZEIDLER, *Nonlinear Functional Analysis and its Applications. I. Fixed-point Theorems*, Springer, Berlin, 1986.
 - [45] P. ZGLICZYNSKI, *Fixed point index for iterations of maps, topological horseshoe and chaos*, *Topol. Methods Nonlin. Anal.*, 8 (1996), pp. 169–177.
 - [46] P. ZGLICZYNSKI, *Computer assisted proof of chaos in the Rössler equations and in the Hénon map*, *Nonlinearity*, 10 (1997), pp. 243–252.
 - [47] P. ZGLICZYNSKI, *Multidimensional perturbations of one-dimensional maps and stability of Sharkovski ordering*, *Int. J. Bifurcations and Chaos*, 9 (1999), pp. 1867–1876.